ON THE QUANTUM EFFICIENCIES OF TWENTY ALKALI HALIDES IN THE 12-21 eV REGION*

Paul H. Metzger**

Aerospace Corporation
El Segundo, California

February 15, 1965

ABSTRACT. Absolute photoelectric yields of twenty alkali halides have been measured, using a rare gas ion chamber to determine the flux distribution of the He_2 continuum between 12.4 and 21.2 eV. In addition, semiquantitative absorption coefficients were obtained by evaporating AX (alkali halide) films on 300 Å thick Al_2O_3 windows. For most of these materials the photoelectric yield rises to values as high as 0.8 electron/incident photon in the fundamental band beyond the stable exciton region. At photon energies near twice the threshold (or approximately 2 E_g) the yield often reaches a distinct minimum of the order of 0.4 electron/incident photon. This region is likely characteristic of double exciton production. Beyond 2 E_g the yield generally rises to very large values, even over 1.0, strongly implying double excitation processes. Many broad diffuse bands, sometimes well correlated with the absorption coefficients, appear in the electron emission spectrum.

*This research supported under NASA Grant No. NsG-328 at the University of Hawaii, Honolulu, Hawaii.

** On leave 1963-64.

I INTRODUCTION

The alkali halides (AX), as a class of materials, are a group of wide band gap insulators, (ranging from 7.0 to 14 eV) whose electronic properties may be studied by use of vacuum ultraviolet techniques. Eby, Teegarden, and Dutton[1] have made measurements of the optical densities of nineteen alkali halides in the 6 to 11 eV region. Several other studies[2,3,4] have been made using photoemission in the "volume" region to deduce thresholds, electron affinities, and other properties of these materials. Recently, these types of measurements have been extended to higher photon energies (12 to 21 eV) using a helium continuum light source whose absolute spectral distribution has been determined.[5,6] The remarkably high yields even in the fundamental band at roughly 5 eV beyond the forbidden gap energy has been explained by Duckett[7] to be consistent with a multi-scattering diffusion process. The present research is an extension of the former work on the halides of Li, Na, and K, with particular attention paid to the absolute intensity calibrations, and complete optical transmission for all twenty alkali halides are presented.

II EXPERIMENTAL

Much of the experimental method has been reported in an earlier paper[7]; however, some details of the calibration procedure will be included here. The light source produced the Hopfield helium continuum with good intensity which was dispersed by a one meter, normal incidence monochromator of the Johnson-Onaka type. The flux distribution of the source as observed at the exit slit is shown in Fig. 1, together with the response characteristics of a platinum photocathode used as a secondary reference for this spectral region.

The primary calibration was done by measuring the photoionization currents for the rare gases argon, krypton, and xenon in the continuous region of their absorption, for which the process, atom + $h\nu$ = ion + e^-, is dominant. Care must be taken to choose experimental parameters such that (1) the pressures are relatively low in order to avoid appreciable recombination of ion pairs and also to assure that the mean free path for electrons is large, (2) the collection efficiency of the chamber is high, maintained by a sufficiently large but not excessive uniform field, (3) secondary effects such as ionization by electron impact, multiple reflections of the primary photon beam, non-uniform gas density are avoided, or made to be small. The arrangement used was a parallel plate ion chamber of long path length (47 cm) attached behind the exit slit of the monochromator. The divergent beam was trapped in a cup shaped photocathode made of platinum, 47 cm from the exit slit. The gas

(A, Kr, or Xe) was introduced into the ion chamber through a micro-leak valve at the end of the chamber and was allowed to flow into the monochromator through the exit slit. Further details of this method are outlined in an earlier paper including cross section measurements of the rare gases.[5] The steady state current i from such an ion chamber is given by:

$$i = eN_o\gamma z\,[1-\exp(-n\sigma L)]$$

where:

e = electronic charge

N_o = number of photons/sec entering ion chamber

γ = ionization yield of the gas

z = charge/ion pair

σ = absorption cross section of the gas in cm^2

n = particle density of gas in cm^{-3}

L = path length in cm

For the rare gases under these conditions, it is probably safe to assume that each photon (absorbed by an atom) of enough energy to produce an ion pair (namely in the ionization continuum above the $^2P^o_{1/2}$ limit) does so without energy degradation into other processes. This is certainly not true of molecular gases above their first ionization potential, where a variety of other channels are available including dissociation. It is therefore assumed that the ionization efficiency of a rare gas atom is 100% or very nearly so, since other processes competing for the same photon are negligible. In fact, recently Samson[8] and Matsunaga et al[9]

have obtained a photoionization yield of unity for xenon in the spectral region 850-1020 Å by means of a thermocouple. Therefore, Eq.(1) may be simplified to

$$i = eN_o[1-\exp(-n\sigma L)] \qquad (2)$$

For large optical densities all of the photons entering the cell are absorbed before they reach the photocathode, and the ion current measured shows the predicted saturation. Under these conditions $i/e = N_o$. There was some question as to whether the saturation curves were actually subject to a systematic error due to recombination at the relatively high pressures necessary to achieve total absorption. It was found that at short path lengths (20 cm) Xe and Kr did not give the same result as argon. As the path length was increased, for the same saturation threshold, first krypton came into agreement with the argon results, and then, for $L > 40$ cm, the xenon results which had previously been low, gave good agreement. Data for all three rare gases are shown in Fig. 1. As a further check, a plot of i/e vs. $[1-\exp(-n\sigma L)]$ should have slope N_o and zero intercept.[5] Data were obtained at low optical densities using calibrated thermocouple gauges to measure the pressure as a function of the ion current. Good agreement with the curve of growth of ion current predicted by Eq.(2) was obtained, and satisfactory agreement with the fluxes obtained by the saturation method was found. The ion chamber was operated with +10 to 15 V across the plates, corresponding to a saturation plateau of the collector current vs voltage characteristics. Only

at photon energies approaching 20 eV did these characteristcs show poor saturation behaviour.[8]

The calibration curves shown in Fig. 1 are the basis of the yield data presented in this report. During the course of the photoemission measurements, re-calibration was repeated periodically (every six days), and it was found that the flux remained constant to within about 4%. Digital readings of the emission current were obtained at approximately 0.1 eV intervals by means of a Benson-Lehner analog to digital reader, and were punched directly into IBM cards. The absolute photoelectric yields of the AX's were computed in two ways:

$$\gamma_1 = \frac{i_{AX}}{eN_o}$$

where i_{AX} = photoemission current from the alkali halide and

$$\gamma_2 = \frac{i_{AX}\,\gamma_{REF}}{i_{REF}}$$

where i_{REF} = photoemission current from the platinum reference photocathode and γ_{REF} = number of electrons per photon from the platinum.

A comparison between γ_1 and γ_2 showed good agreement, in spite of the fact that the Pt photocathode was re-cycled to air two or three times a day after being under vacuum conditions during measurements. Apparently, whatever surface contamination that the platinum might have had did not appreciably alter the response characteristic as long as the Pt was not subjected to extreme conditions.

The experimental chamber was quite similar to that described in an

earlier report[7] except for the following changes. The vacuum system was pumped by a liquid N_2 baffled 4-inch diffusion pump, allowing lower pressures to be maintained during evaporation. A Sloan model DTM-2A, layer-thickness monitor was used to obtain semiquantitative film thicknesses. The sample holder was arranged so that the rotation and translation axis was orthogonal to the beam direction, allowing measurements of photocurrent as a function of angle of incidence to be made.

Data were obtained in the following manner. The AX's were loaded into pre-fired molybdenum boats and outgassed below their melting points in vacuum for several hours before evaporation. After vacuum conditions reached the 10^{-6} Torr range a nickel-coated microscope slide substrate was moved into position adjacent to the quartz crystal oscillator head of the DTM-2, with the Ni coating facing the evaporation source. The AX always melted sharply, the liquid melt being observed through a lucite flange on the system. At this point the shutter directly below the nickelized substrate was opened, and almost immediately the DTM-2 began to respond. From a previous experiment of film thickness versus photocurrent, it was found that the emission current reached saturation for relatively thin films of only a few hundred Angstroms thickness and remained essentially constant for the thickest films of about 5000Å. An optimum thickness of 2500Å was chosen. The electron collector plate was maintained at 45 V positive relative to the photocathode. Before evaporation the electron emission current was measured from the nickel substrate, which was lower, in general, by at least a factor of three than the AX. Data were obtained

with the AX cathode at both $+45^{\circ}$ and -45° incidence to the beam as well as at normal incidence. The current was usually some 20% higher at the inclined angles and was a minimum at normal incidence as might be expected. Most of the data shown were obtained at 45° incidence with a relatively unpolarized beam. Repeated measurements were made with the beam at different locations on the AX film as well as with different films. The photocurrent from the Pt reference cathode was recorded both before and after the AX measurements by pulling the rotary feedthrough out and allowing the beam to fall on the Pt, some 25 cm behind the AX sample and well protected from the evaporation unit.

Transmission data were obtained as described earlier[7] by evaporating the AX's on 300 Å thick self-supporting Al_2O_3 films. An open photomultiplier manufactured by IT and T was altered by evaporating CsCl onto its photocathode, which improved the overall gain for this spectral region, and made it a good detector for the transmitted light which was small. However, it was necessary to prepare fresh photocathodes after a couple of exposures to air due to the uptake of water vapor by the CsCl. The primary yield of CsCl in this region is 0.6 electron per incident photon or greater. There is an annoying peak at 13.2 eV which adds to the uncertainty of any structure found in that region for the AX's. The absorption coefficients, α, were computed and plotted by a Cal-Comp plotter.

III RESULTS

Absorption coefficients, shown by the solid curves in Figs. 4a-t may be defined through the relation $N = N_o \exp(-\alpha t)$, where N_o and N are the number of incident and transmitted photons/sec, respectively, and t is the film thickness in cm. The α's are only semiquantitative and represent order of magnitude coefficients due to the large uncertainty in measuring thicknesses t. Since these coefficients are roughly 10^6 cm^{-1}, 100 Å films gave about 37% transmission. No corrections were made for reflectivity, which in some cases is appreciable and may account for slight shifts in the band positions. Data were collected for light transmitted both directions through the film; that is, in the first case the light entered the AX first and then the Al_2O_3 and in the second case the reverse order was true. In most cases no real difference was observed. The obvious point to be seen from the curves shown in Figs. 4-23 is that there is some correlation between the absorption coefficient curves and the photoemission curves (dotted lines).

The present results are in good agreement with our earlier results at the long wavelength end of the spectrum, but a systematic deviation was found at the short wavelengths, particularly for wavelengths shorter than 750 Å. It is suspected that the Pt calibration formerly used was in error since it had not been re-checked against the ion chamber for some time. It should be noted that some of the yields are greater than unity, particularly for the narrower band gap materials. Further, it should be noticed

that these high yields, reaching values greater than unity, only occur at energies greater than twice the band gap. The bands observed in photoemission are somewhat more diffuse and shifted to higher energies compared to the corresponding bands in the transmission data. Most of the structures seen in Figs. 4a-t are even quite obvious in the raw data, since the light source background is continuous. An example of the raw data may be seen in Fig. 2 and 3, in which i_{REF} is the photoemission from the reference cathode and i_{AX} is the emission current from the alkali halide.

IV DISCUSSION

Fig. 5 shows idealized absorption and photoemission spectra for a typical AX. For most AX's the first two exciton peaks are usually non-degenerate with the interband scattering continuum. An exception to this appears to be LiF (see Fig. 4a) in which the first exciton peak near 13 eV shows a corresponding photoemission peak. Beyond the stable exciton region there is usually an absorption shoulder corresponding to the onset of interband transitions, followed by (~ 1.0 eV greater energy) the onset of strong electron emission, the threshold of which is labeled E_g in Fig. 24. There appear to exist several diffuse absorption and photoemission bands which have been identified as metastable exciton transitions.[10,11] In the photoemission spectrum the absolute yield is seen to rise to a maximum of the order of 0.8 photoelectron/incident quantum roughly 5 eV past the threshold E_g. This fundamental band, due to the onset of band to band transitions, shows some structure, depending on the density of states, and also is correlated with the absorption coefficient showing distinct correlation with the metastable exciton peaks. Some notable examples of this are CsCl and CsBr with peaks at 13.2 eV and CsF at 12.9 and 13.8 eV. As the energy of the photon probe is increased, the photoelectric yield declines to roughly half of the peak value in the fundamental band reaching a distinct minimum, in most cases, near 2 Eg. The photoyield appears to drop more readily than the optical absorption would predict. There is a strong implication that a process in which

the primary photon excites two excitons rather than a single fast photoelectron, becomes important in this region. In fact, Miyakawa[12] has suggested that the cross section for this process may be quite large. Newburgh[4] has shown from retarding potential measurements that the distribution of emitted photoelectron energies suddenly decreases at photon energies of 2 E_g and greater. This is consistent with a single photon producing two slow electrons near 2 E_g. Beyond 2 E_g the yield rises again, implying that exciton ionization again is dominant. It should be noted that the yield beyond 2 E_g often reaches values of 1.0 or greater (as opposed to $\sim$0.8 or less in the fundamental band) suggesting that a secondary process is occuring. The emission from the p^5 halide valence bands (F^-, Cl^-, Br^-, I^-) probably dominate the observed interband continua, but the deeper lying cation levels may become important around 20 eV. A further process which may occur in the high energy spectrum is the ionization of impurity levels by fast photoelectrons, a two for one process which could contribute to the high yield in this region. Table I summarizes the 2 E_g minima observed and compares them to the results of other workers. It is interesting to note that all of the materials showing well-developed minima are just those which have good absorption shoulders, according to the data of Eby *et al.*[1]

The observed optical minima are relatively more uncertain, but the minima corresponding to twice the forbidden threshold seem to be at twice the observed absorption shoulder edges listed in Table I.

Photoemission minima seem to "lag" the optical minima by an amount proportional to the electron affinity.

Since no corrections were made for reflectivity, it is somewhat tentative to list peak and valley positions with any degree of accuracy. In spite of this, there seems to be fairly good correlation between the absorption and photoemission spectra. In some cases distinct optical absorption in the continuum region appears to have no counterpart in the emission spectrum, especially near 2 E_g which may be further evidence for the existence of metastable excitons well into the continuum.

The data given by Phillips[4] is in fair agreement with the results shown in Fig. 4. The simple band model shown in Fig. 5 indicates the general features to be identified with the spectra shown in Fib. 4. A more comprehensive treatment of the band structure for the alkali halides is given also by Phillips[13-15]. The peak of the "fundamental" band some 5 ev higher energy than E_g are identified as $X_5' \rightarrow X_1$ transition[13].

V SUMMARY

The photoemission and absorption spectra of the alkali halides show many diffuse bands often well correlated. The electron emission continuum shows a distinct peak and often a well defined minimum at $\sim 2\ E_g$. The magnitude of the quantum efficiencies at photon energies greater than $2\ E_g$ implies multiple processes are dominant.

Table 1. Comparison of observed threshold energy (in eV) with previous data. Values in ( ) are doubtful or rough estimates.

	I $2E_g$ observ.	II E_g	III Absorption Shoulder[a]	IV Threshold[b] ($\gamma < 10^{-3}$)	V Electron Affinity[c], ΔE
FLUORIDES					
LiF	>20	>10	~14[d]		
NaF	>20	>10	>11		
K F	>20	>10	10.9	10.4	
RbF	(18.5)	(9.25)	10.4		
CsF	(15.2)?	(7.60)?	10.0		
CHLORIDES					
LiCl	>20	>10	>10		
NaCl	19.0	9.50	8.60	8.50	0.90
K Cl	18.3	9.15	8.50	8.70	0.65
RbCl	17.2	8.60	8.20		0.40
CsCl	14.8	7.40		(7.50)	
BROMIDES					
LiBr	19.0	9.50	(9.30)		(0.20)
NaBr	16.2	8.10	7.70		0.40
K Br	16.1	8.05	7.80	8.12	0.25
RbBr	15.7	7.85	7.70		0.15
CsBr	14.6	7.30		(7.20)	
IODIDES					
LiI	15.8	7.90	5.90	7.30	2.00
NaI	14.6	7.30	5.80	7.30	1.50
K I	14.0	7.00	6.20	7.30	0.80
RbI	14.4	7.20	6.10	7.30	1.10
CsI	14.1	7.05	6.30	6.40	0.75

a. Reference 1
b. Reference 2
c. Column II minus column III.
d. A. Milgram and M. P. Givens, Phys. Rev. 125, 1506 (1962).

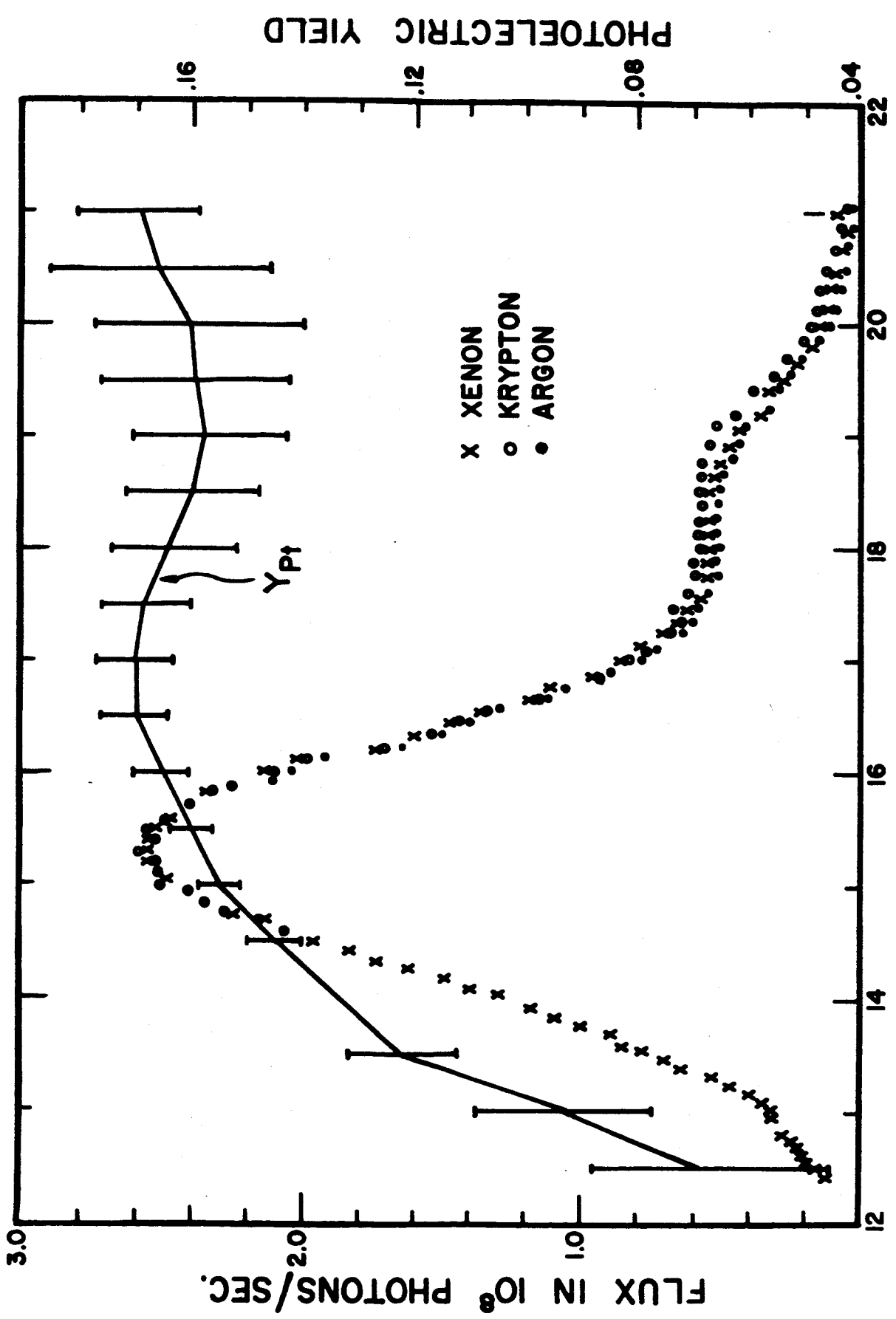

Fig. 2 Photon flux at the exit slit and photoelectric yield of a platinum detector

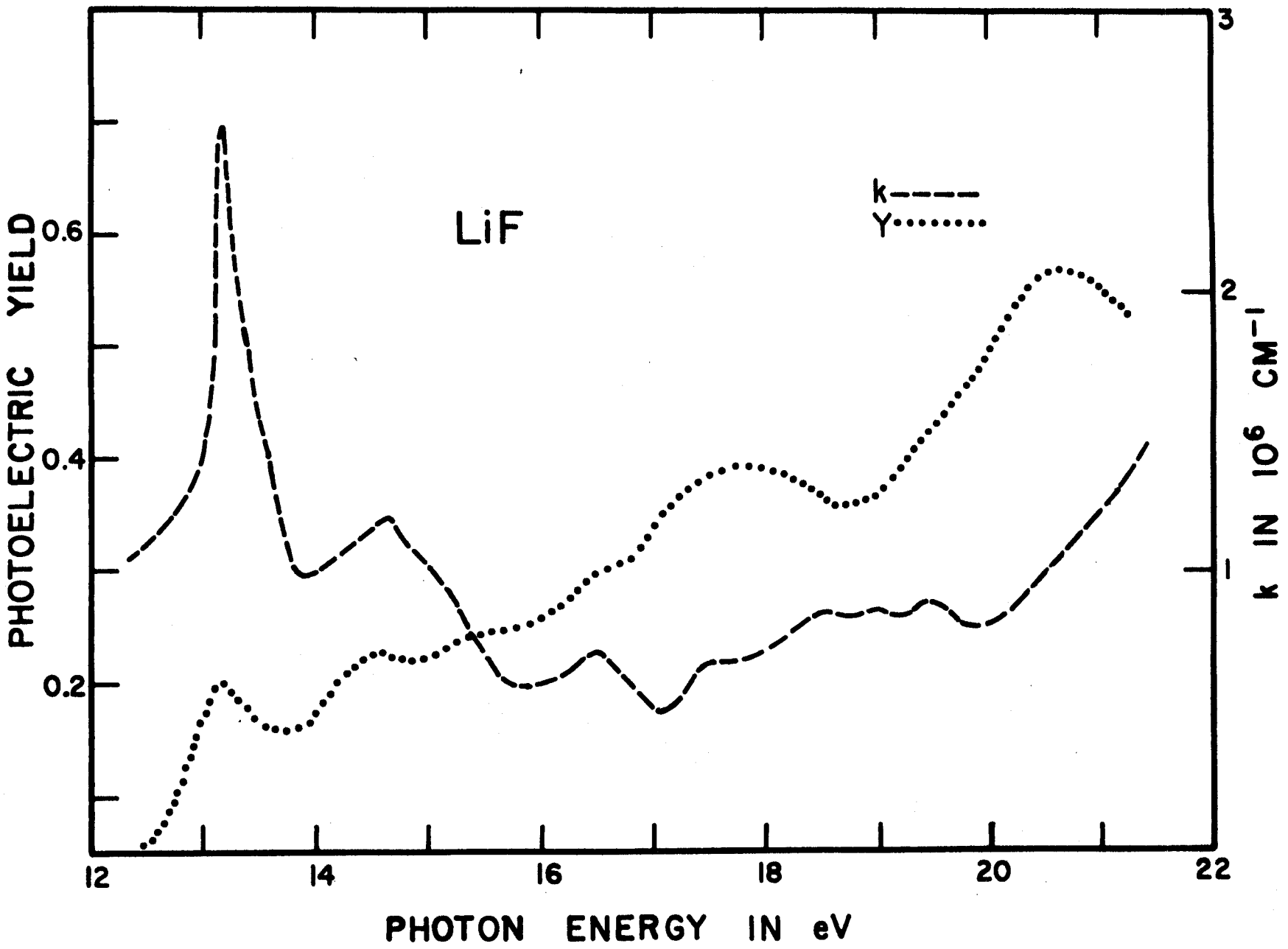

Fig. 3 Photoelectric yield and absorption coefficient of LiF

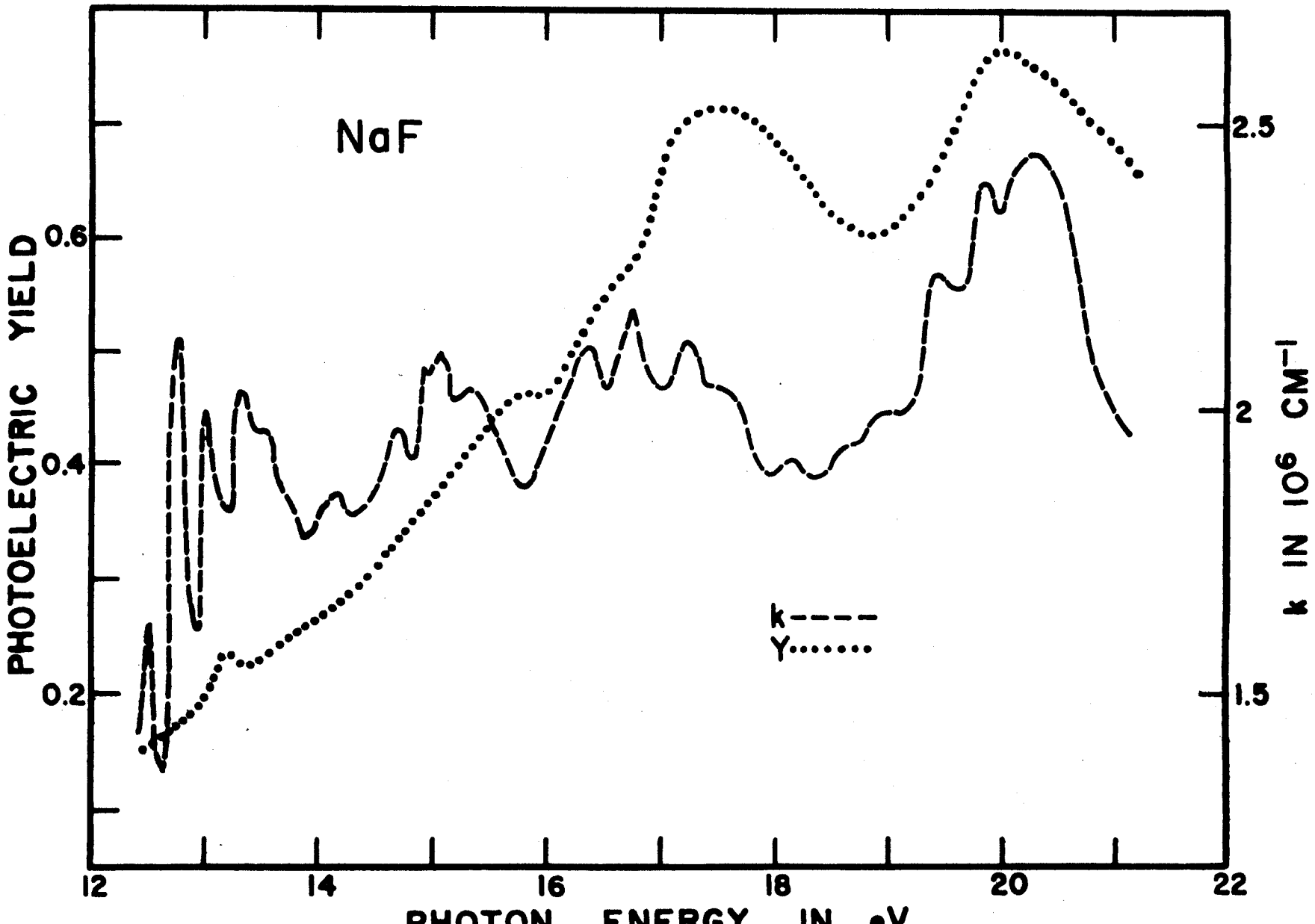

Fig. 4 Photoelectric yield and absorption coefficient of NaF

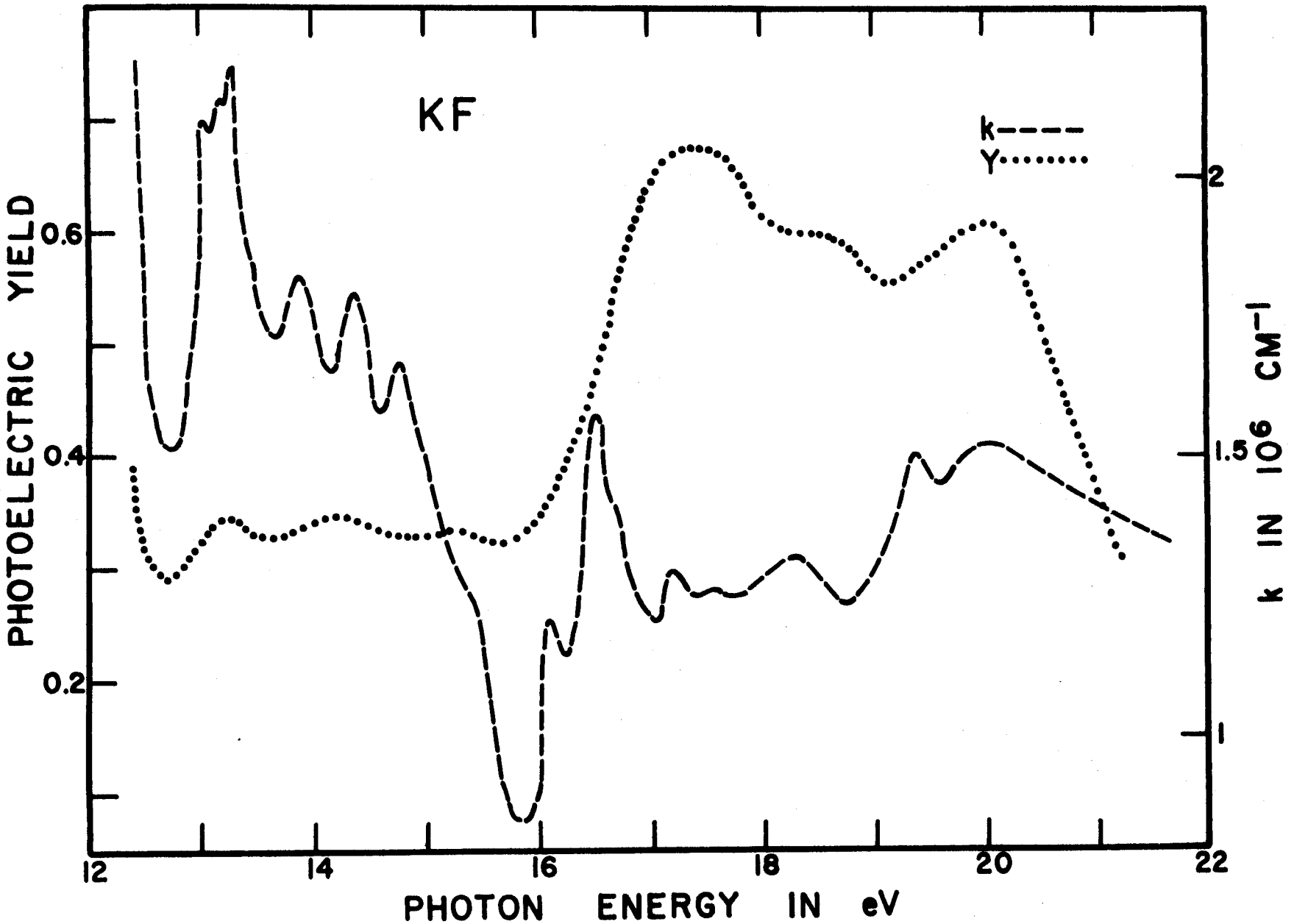

Fig. 5 Photoelectric yield and absorption coefficient of K F

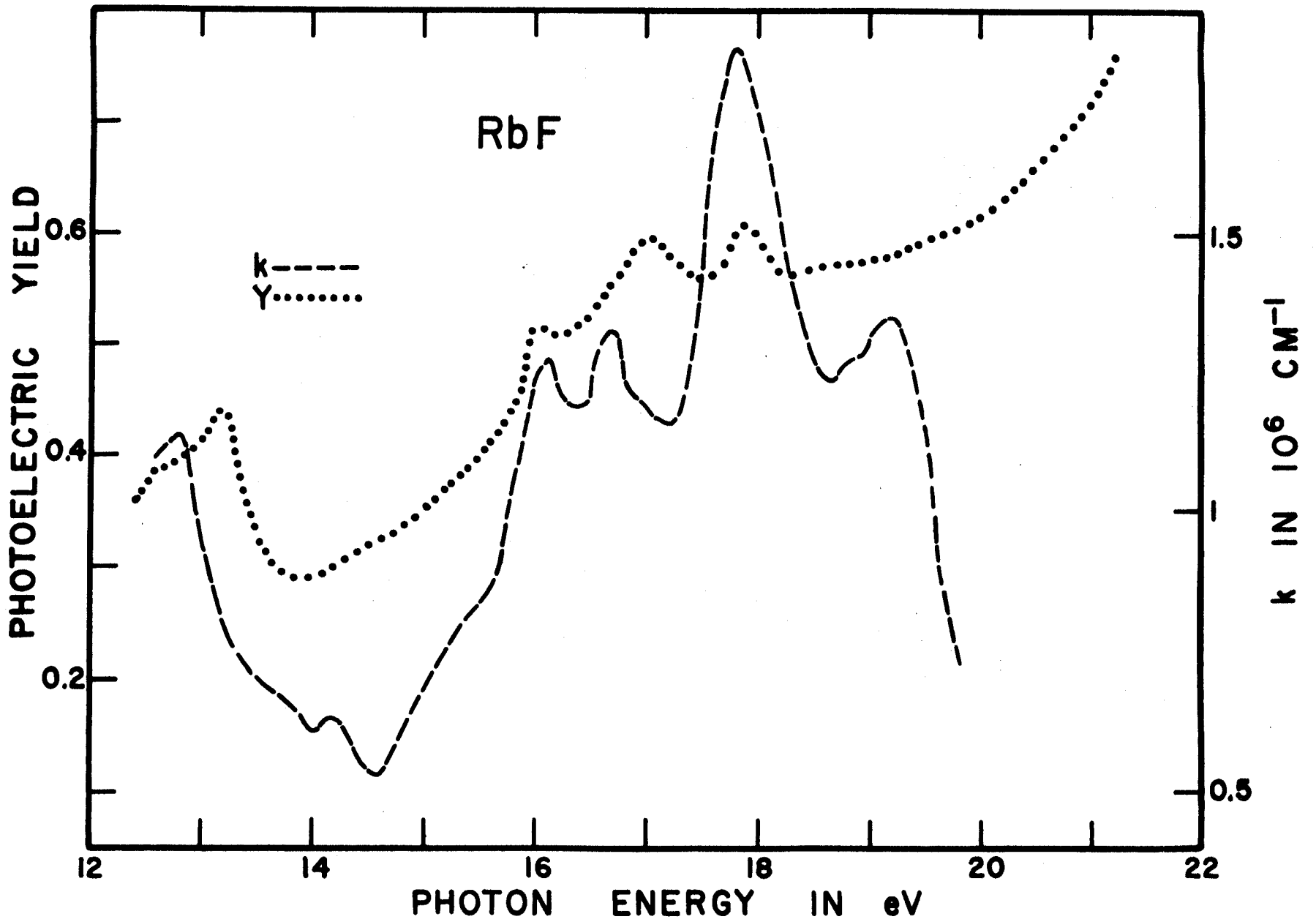

Fig. 6 Photoelectric yield and absorption coefficient of RbF

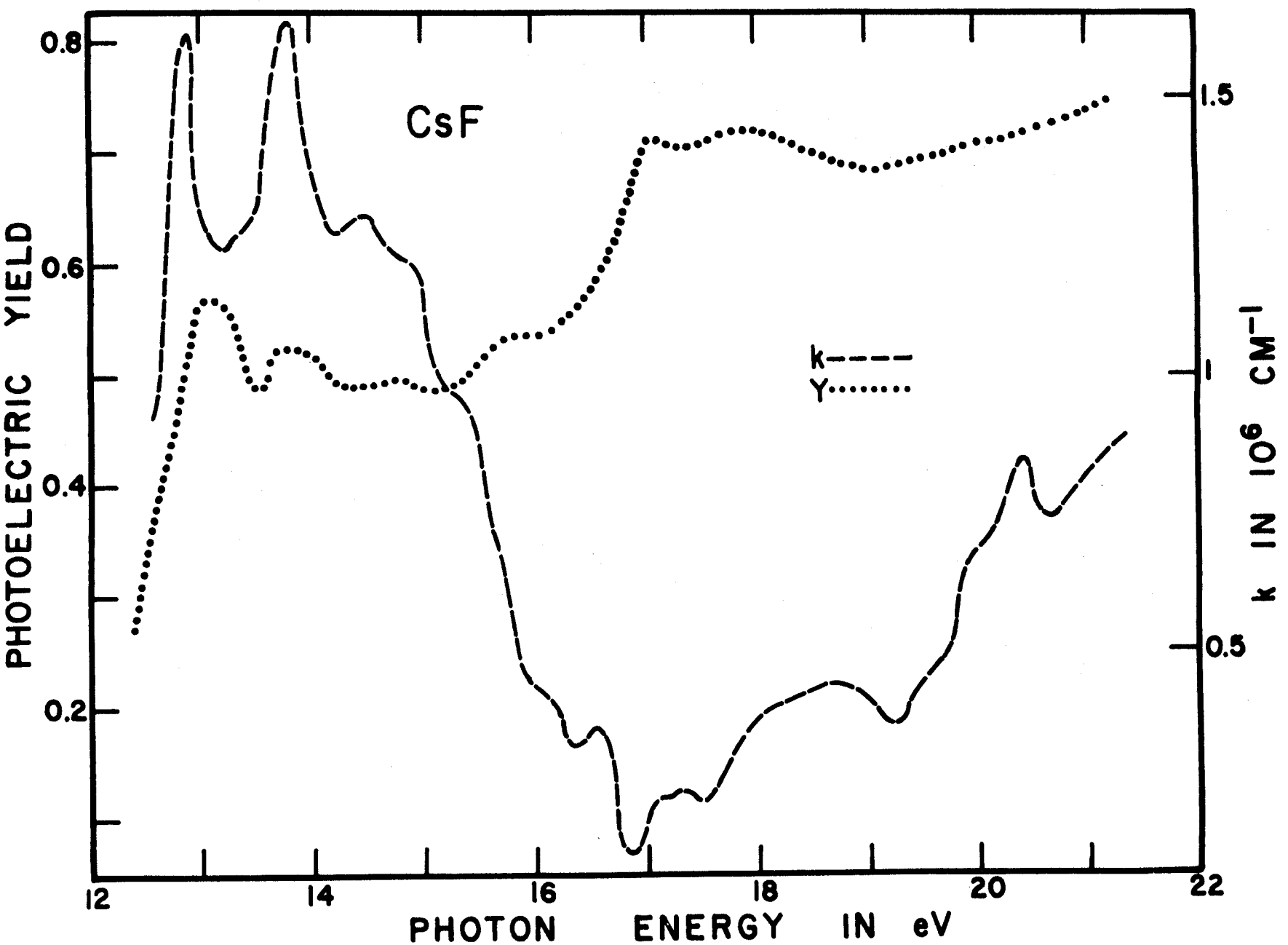

Fig . 7 Photoelectric yield and absorption coefficient of CsF

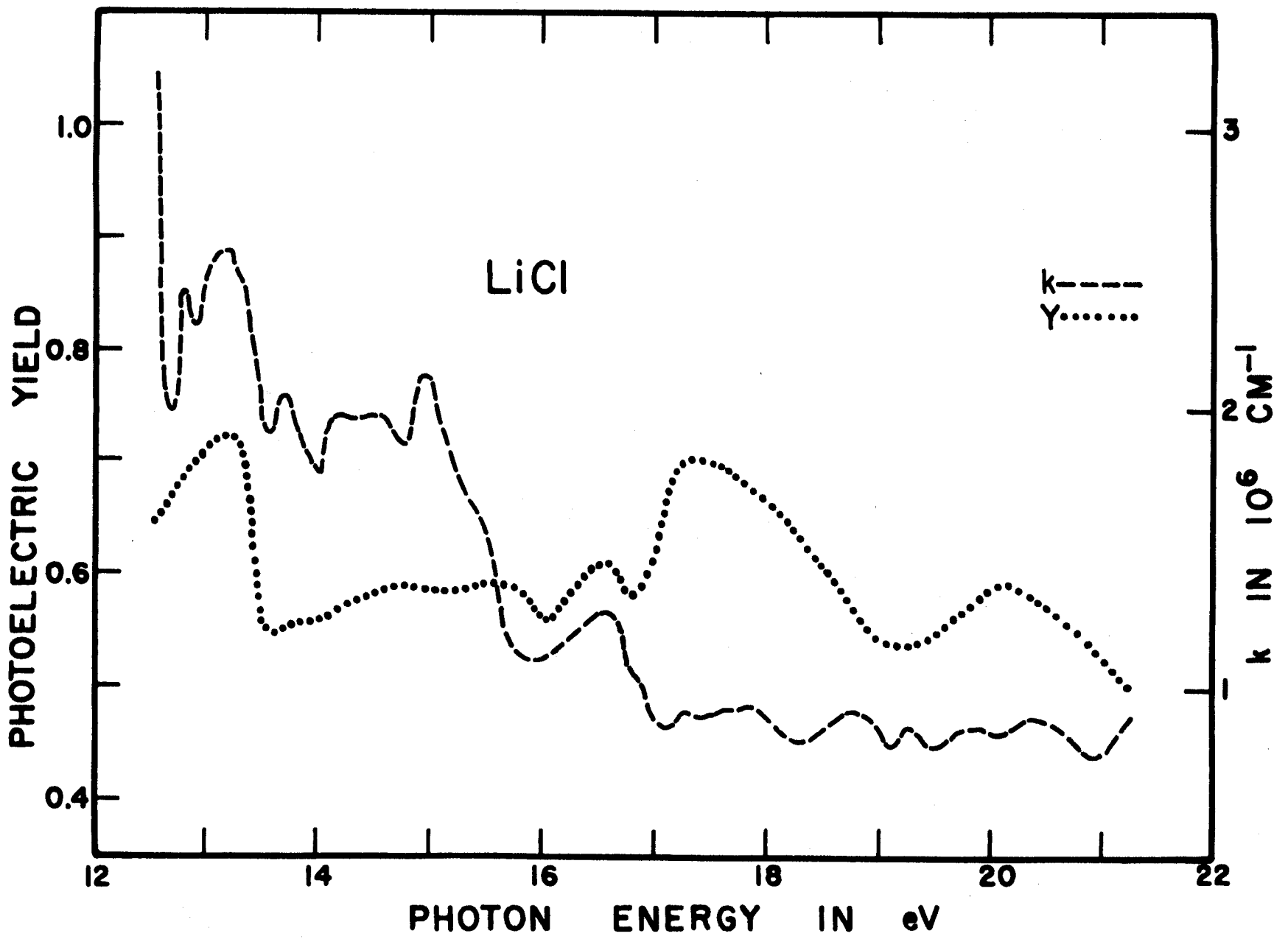

Fig. 8 Photoelectric yield and absorption coefficient of LiCl

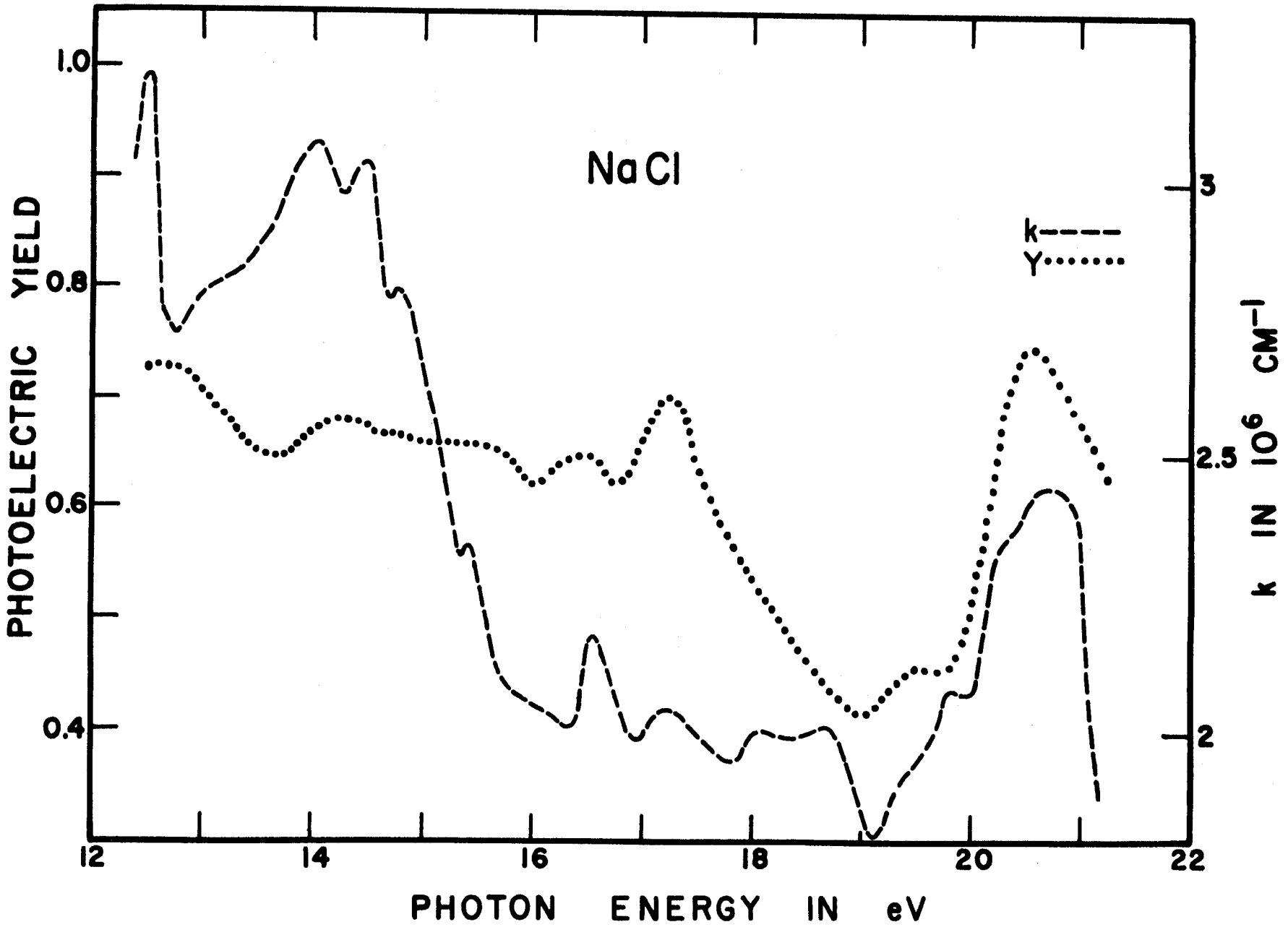

Fig. 9 Photoelectric yield and absorption coefficient of NaCl

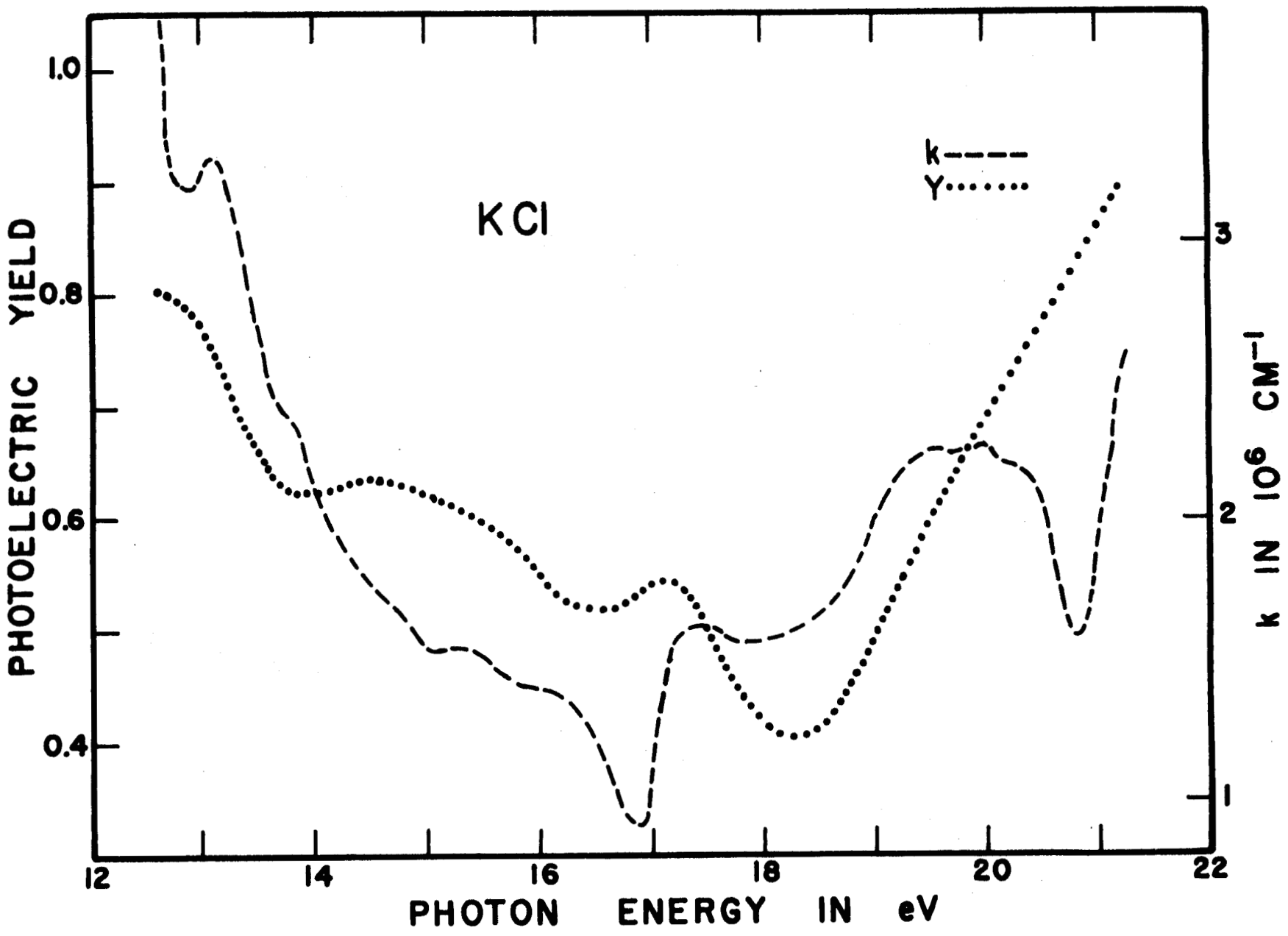

Fig. 10 Photoelectric yield and absorption coefficient of K Cl

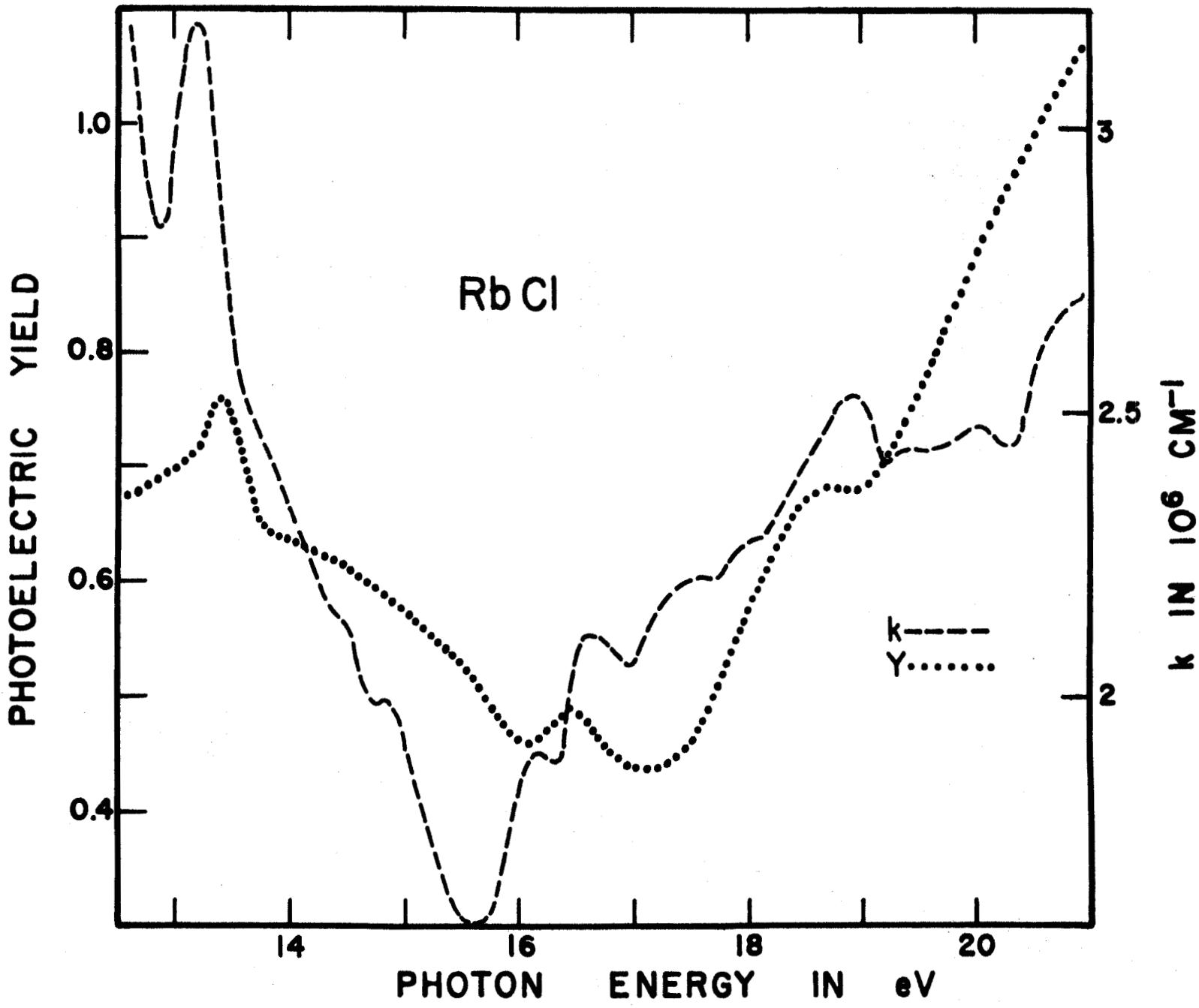

Fig . 11 Photoelectric yield and absorption coefficient of RbCl

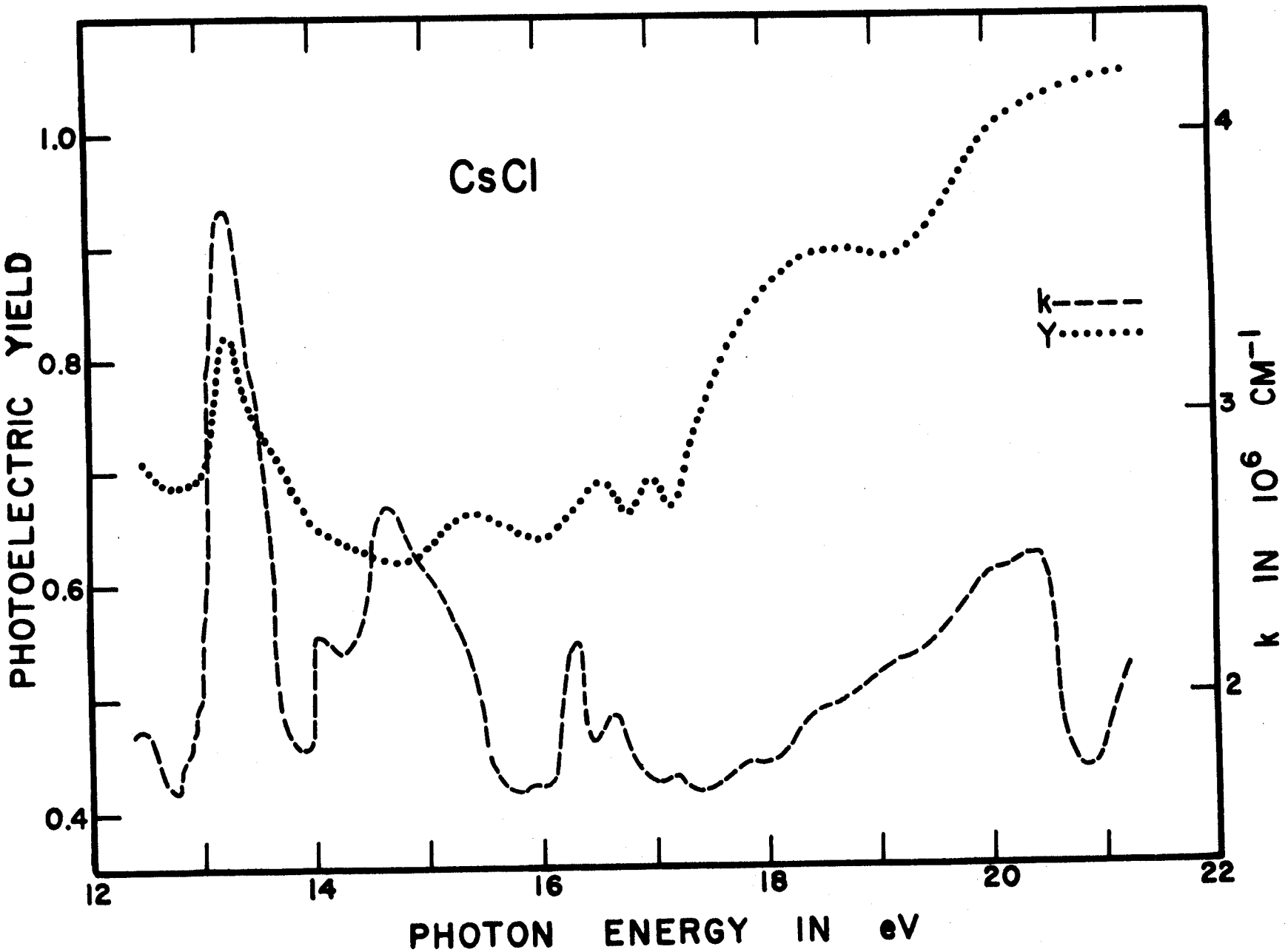

Fig. 12 Photoelectric yield and absorption coefficient of CsCl

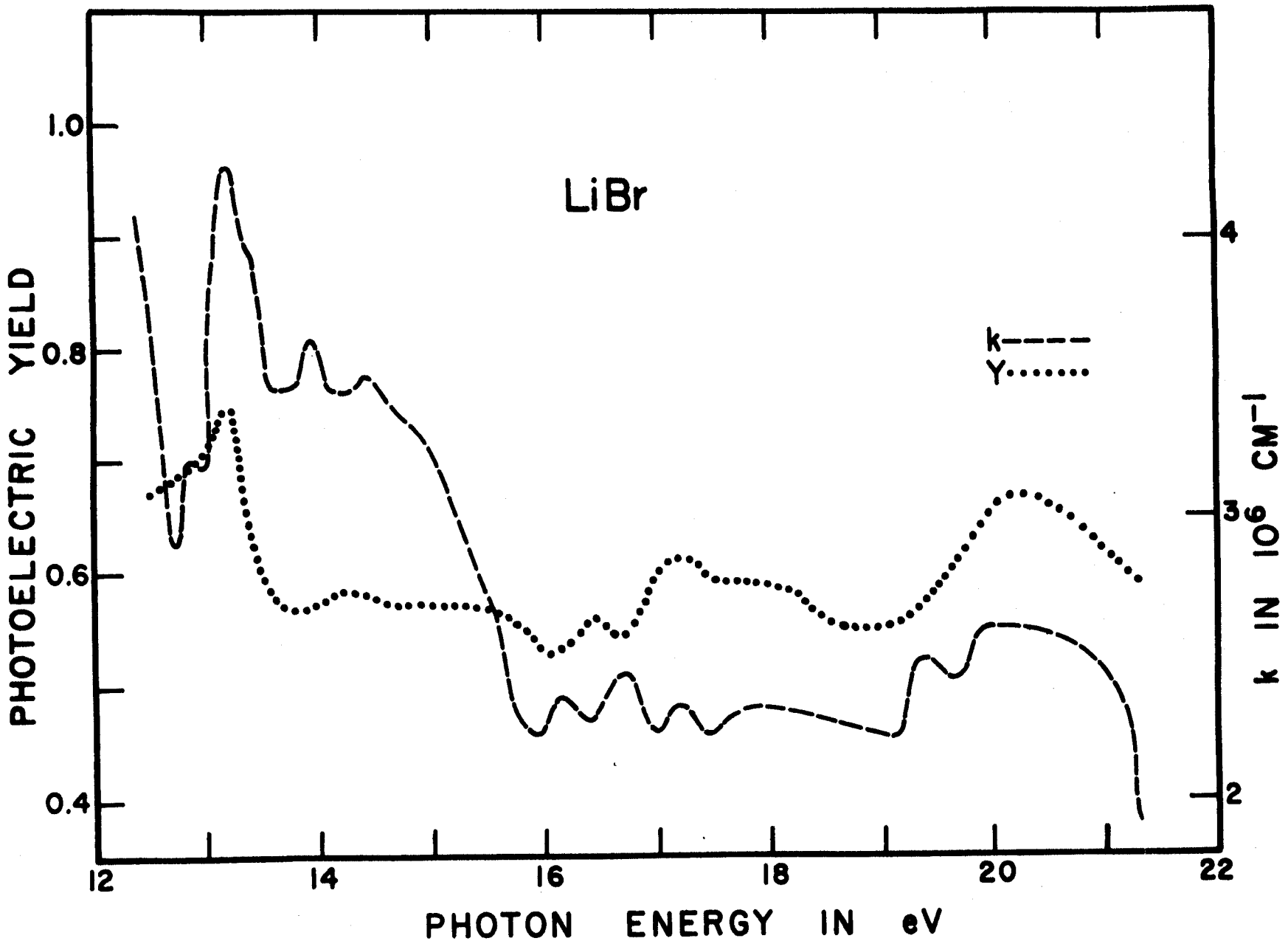

Fig. 13 Photoelectric yield and absorption coefficient of LiBr

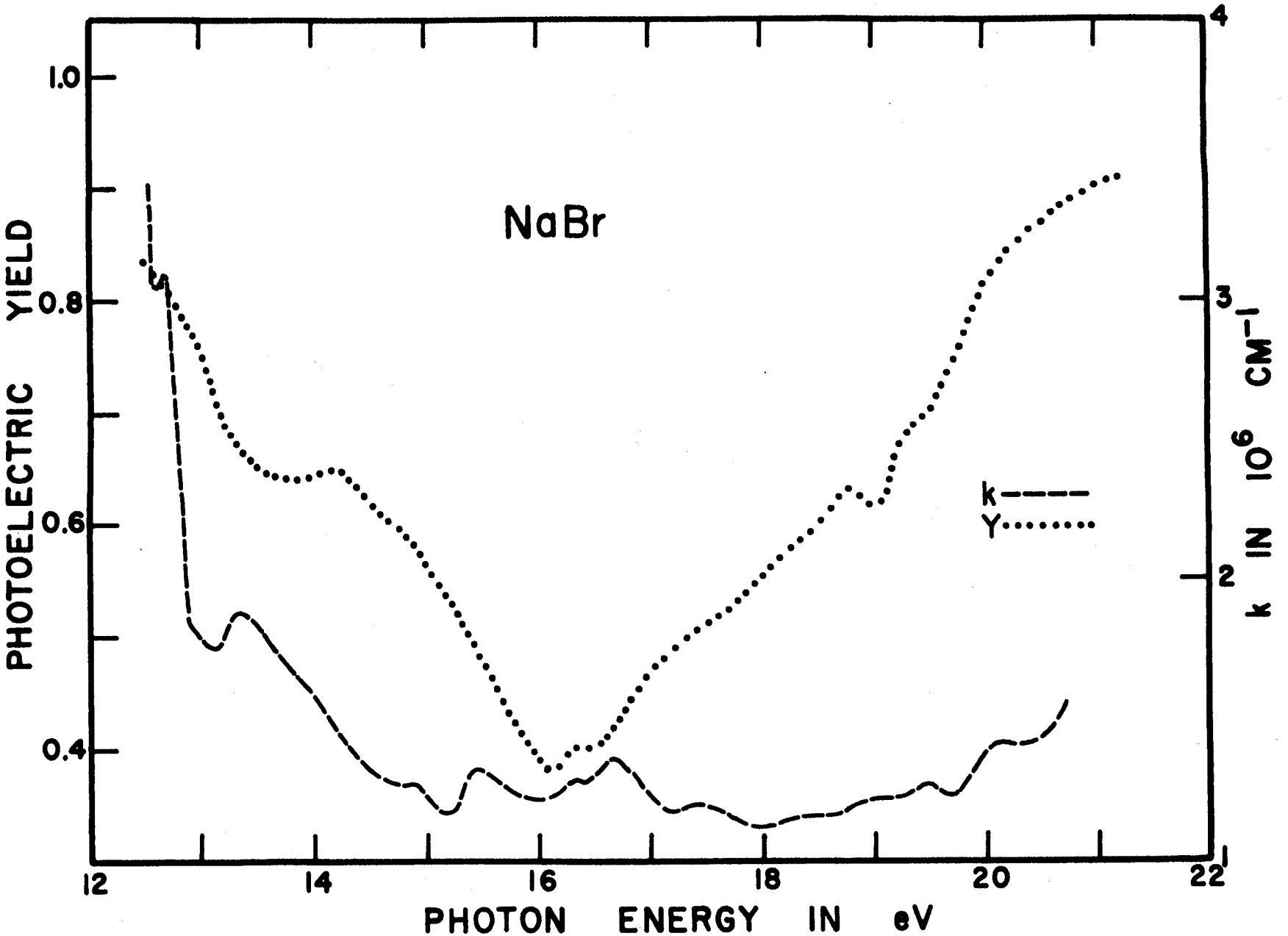

Fig. 14 Photoelectric yield and absorption coefficient of NaBr

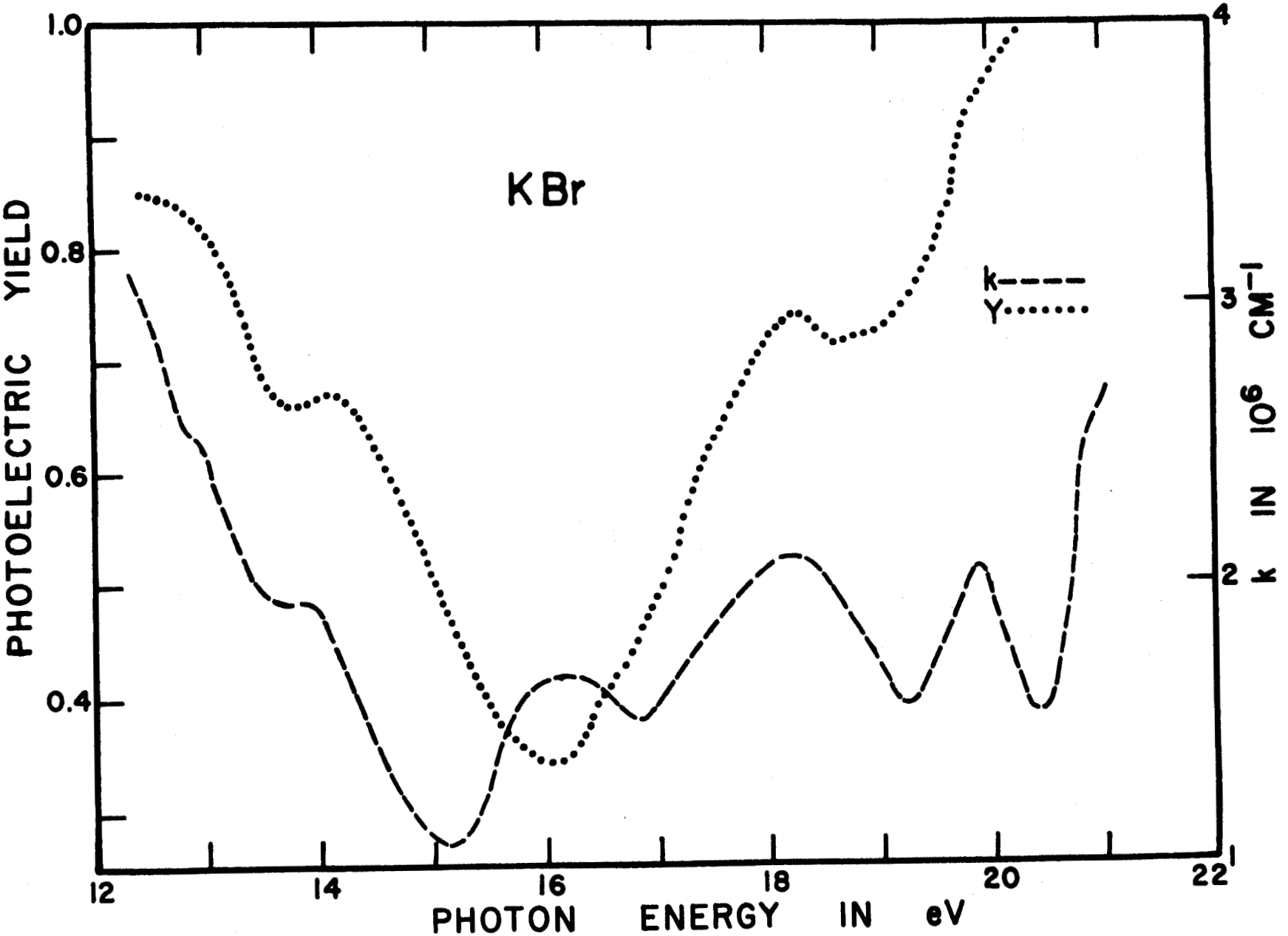

Fig. 15 Photoelectric yield and absorption coefficient of K Br

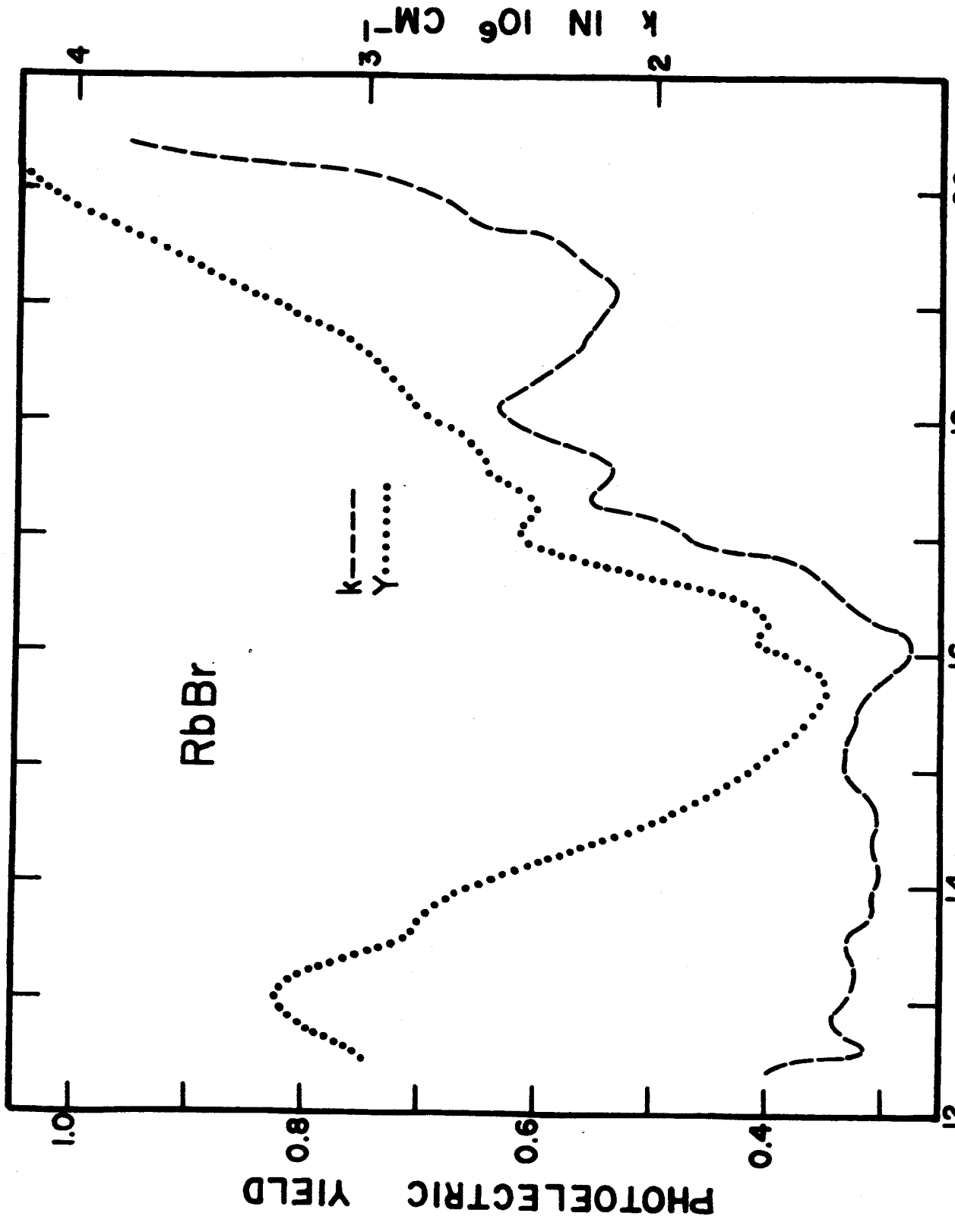

Fig. 16 Photoelectric yield and absorption coefficient of RbBr

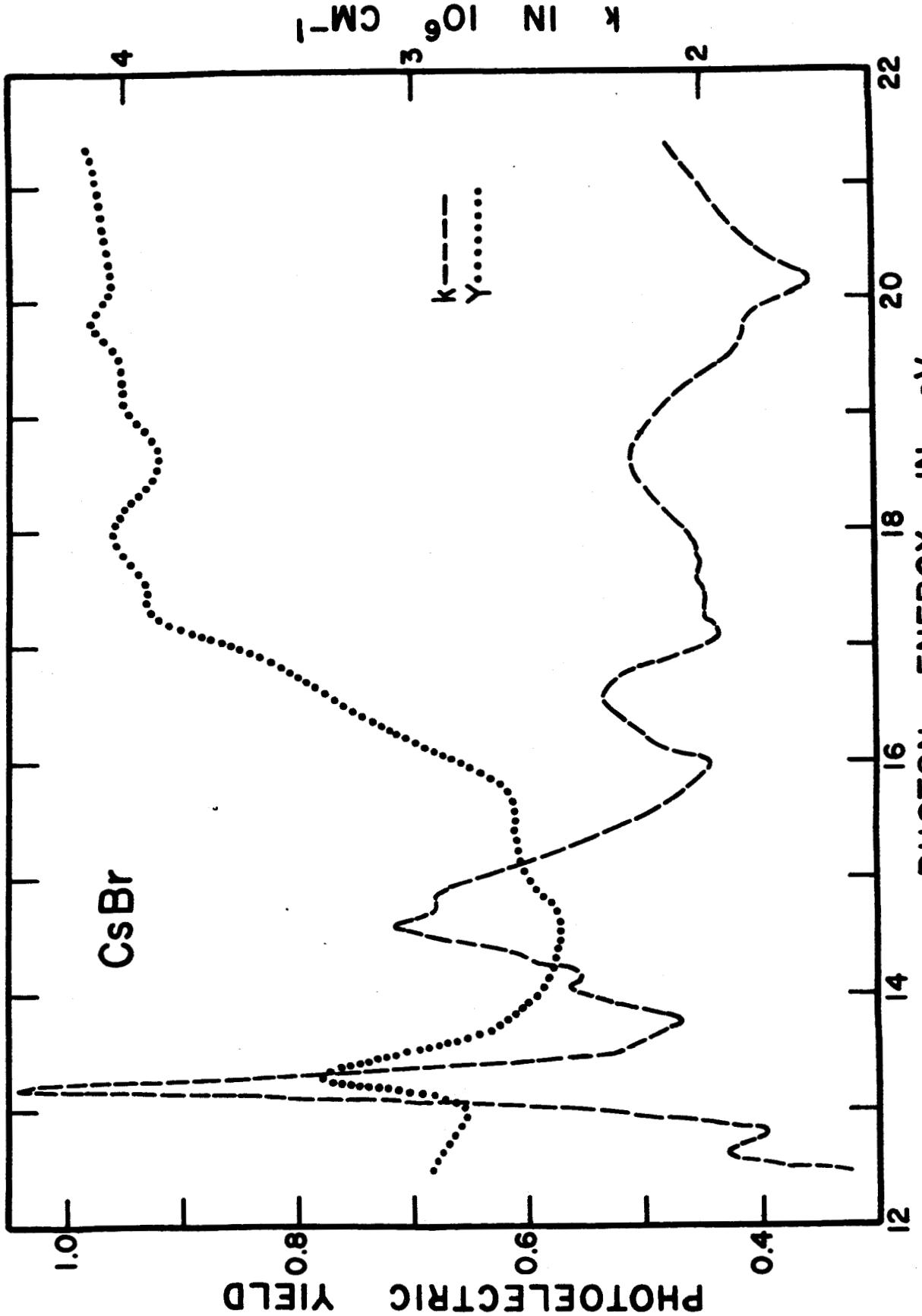

Fig. 17 Photoelectric yield and absorption coefficient of CsBr

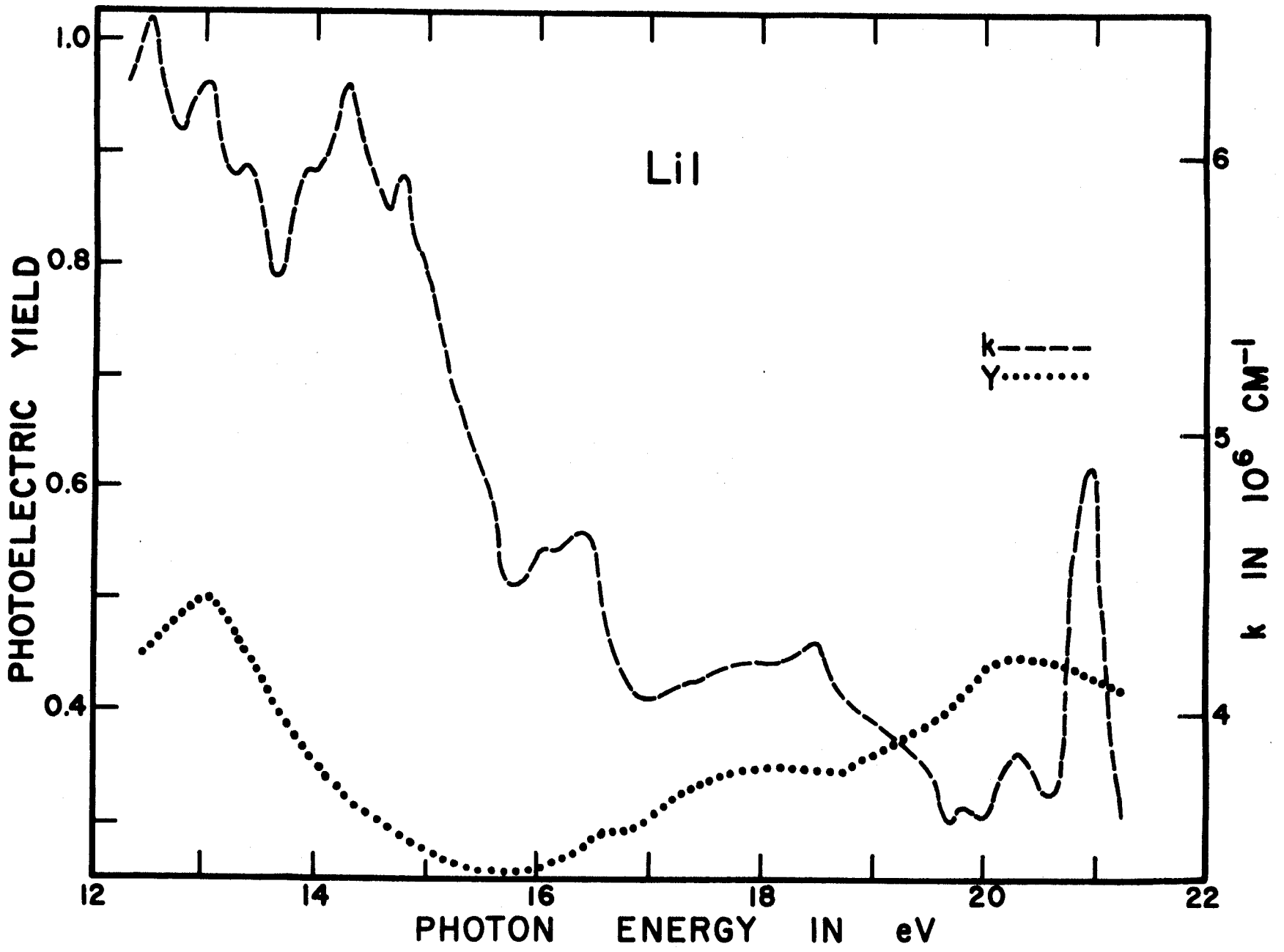

Fig. 18 Photoelectric yield and absorption coefficient of LiI

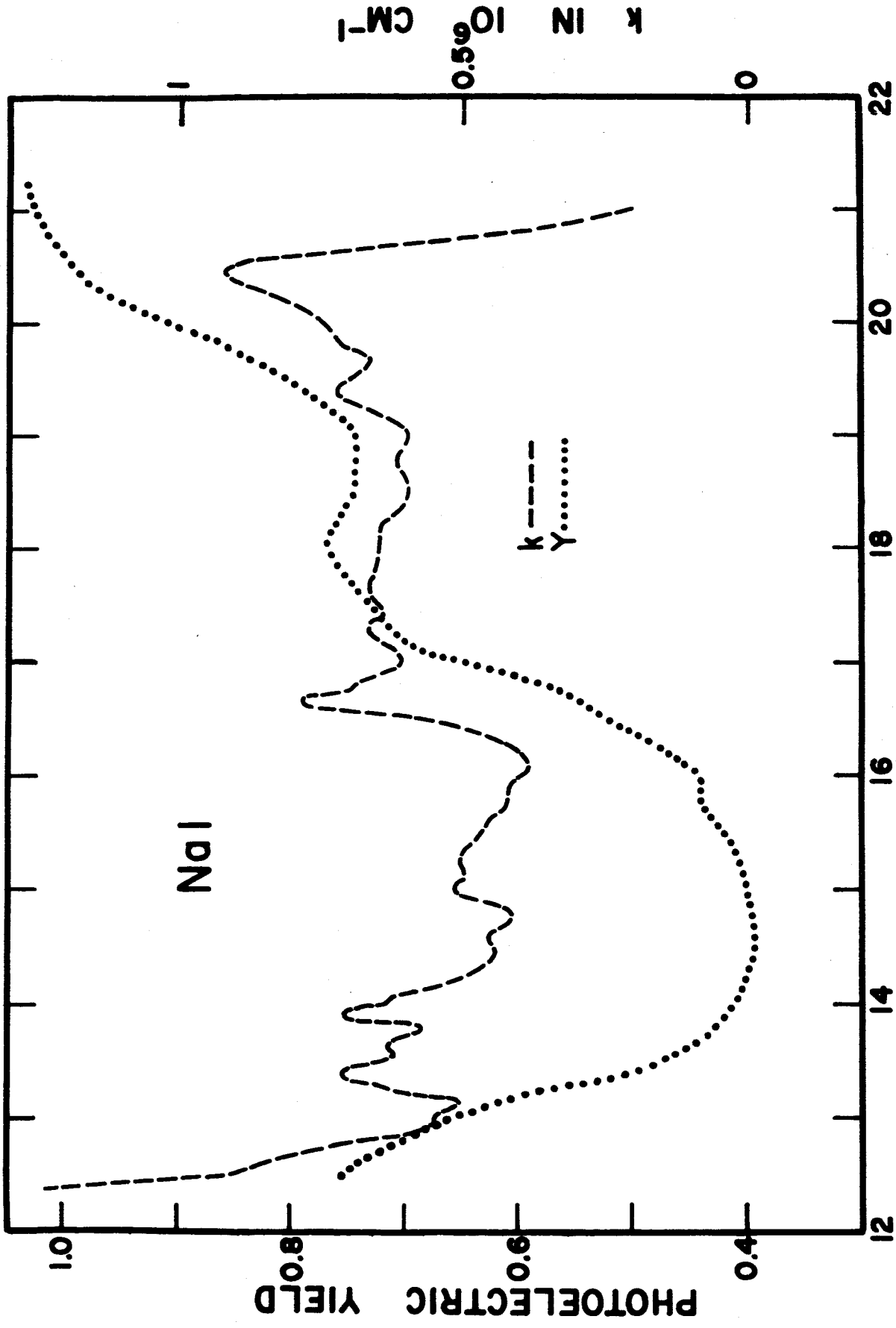

Fig. 19 Photoelectric yield and absorption coefficient of NaI

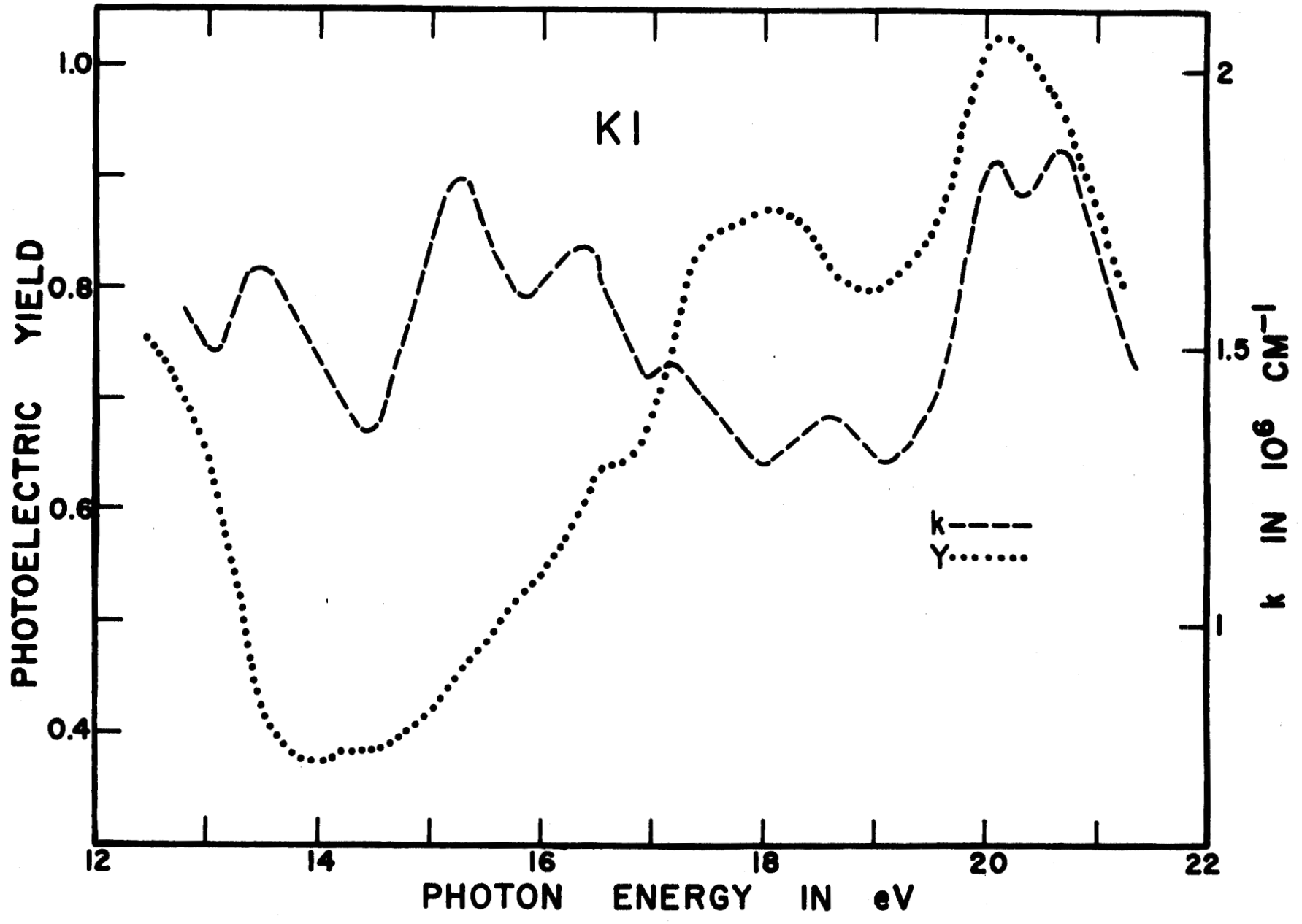

Fig. 20 Photoelectric yield and absorption coefficient of K I

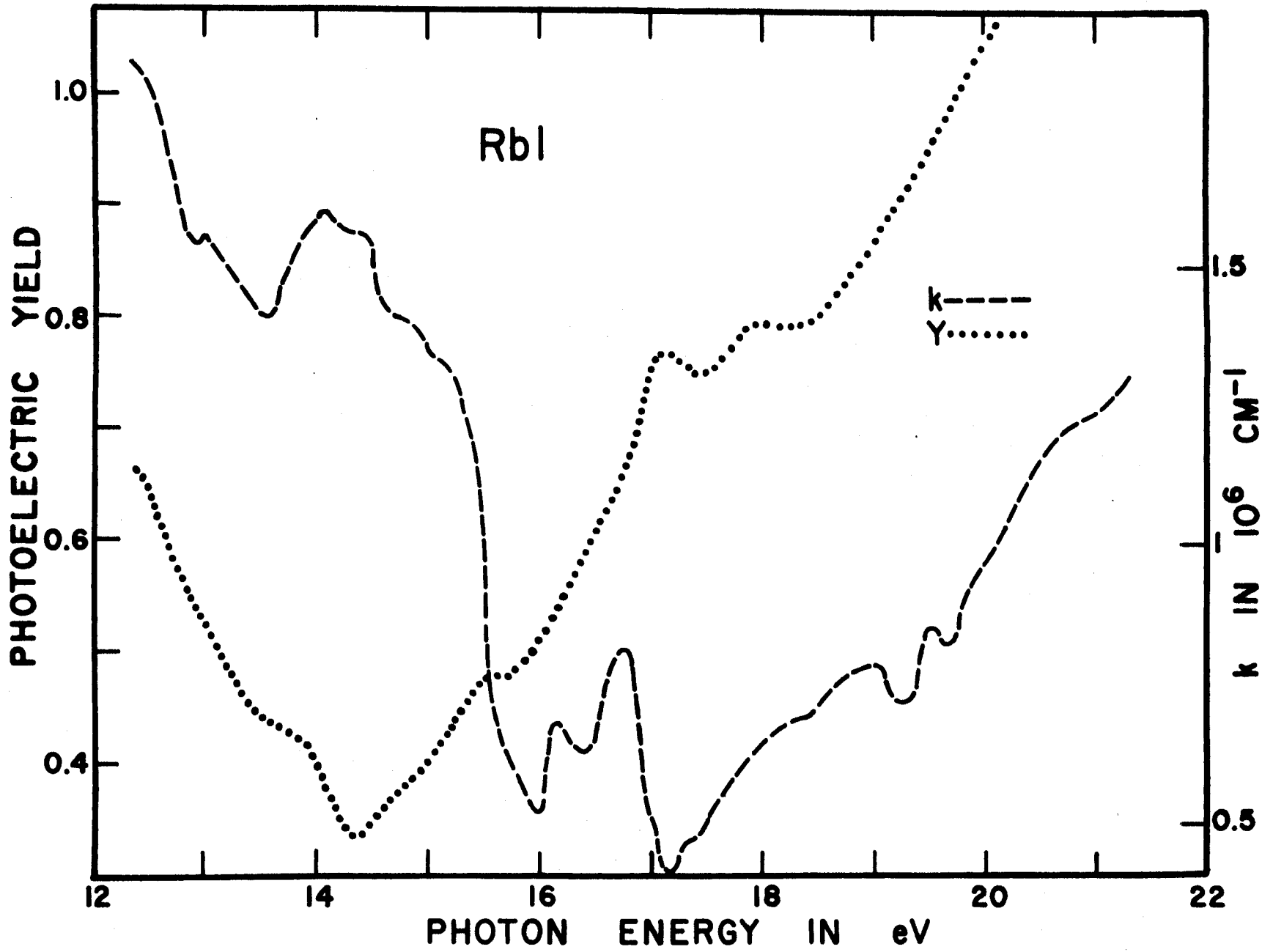

Fig . 21 Photoelectric yield and absorption coefficient of RbI

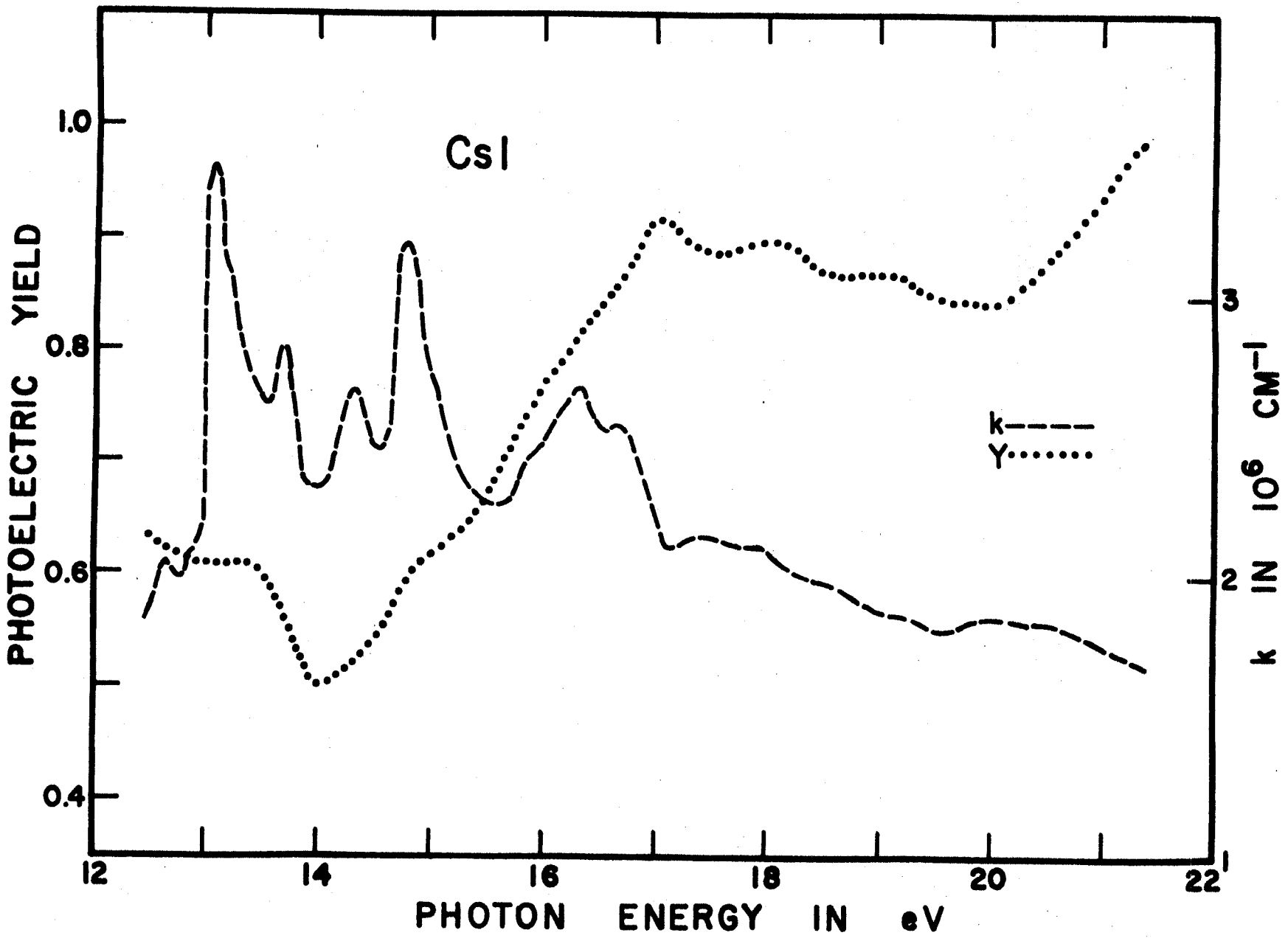

Fig. 22 Photoelectric yield and absorption coefficient of CsI

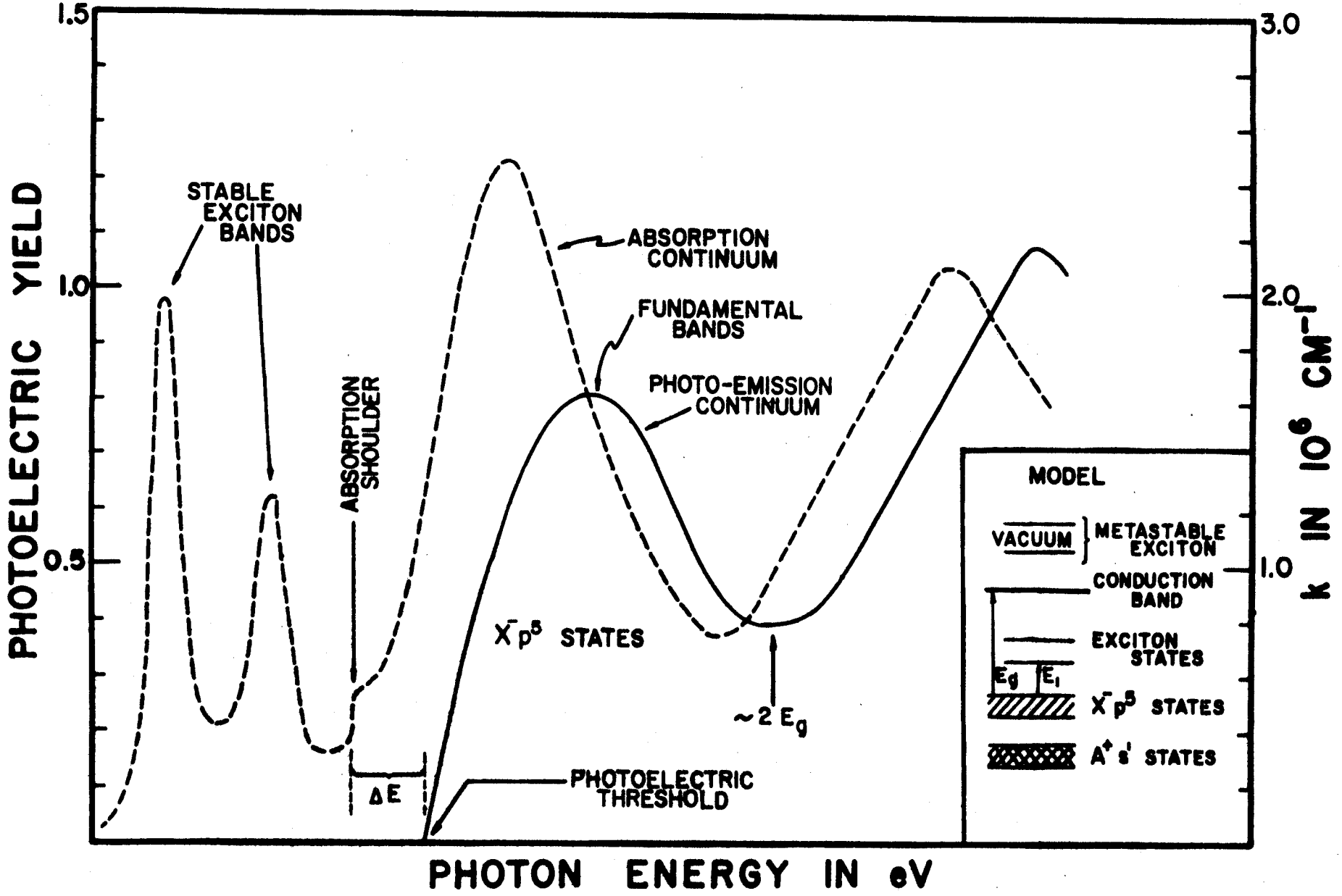

Fig. 23 Idealized absorption and photoemission spectra of an alkali-halide

ACKNOWLEDGEMENTS

The author would like to thank Dr. R. A. Becker and Professor K. Watanabe for the opportunity to complete this work and Professor Wm. Pong for many helpful discussions of it. Also, to the Aerospace Corporation for a fellowship, many thanks are due.

REFERENCES

1. J. E. Eby, K. J. Teegarden, and D. B. Dutton, Phys. Rev. 5, 1099 (1959).
2. E. A. Taft and H. R. Philipp, J. Phys. Chem. Solids 3, 1 (1957).
3. J. W. Taylor and P. W. Hartman, Phys. Rev. 6, 1421 (1959).
4. R. G. Newburgh, Phys. Rev. 4, 1570 (1963).
5. P. Metzger and G. R. Cook, Aerospace Report ATN-63(9218)-2 (to be published. J. Opt. Soc. Am.).
6. G. R. Cook and P. Metzger, J. Chem. Phys. 41, 321 (1964).
7. S. W. Duckett and P. Metzger, Aerospace Report ATN-64(9233)-3; Phys. Rev. (in press).
8. J. A. R. Samson, J. Opt. Soc. Am. 54, 6 (1964).
9. F. Matsunaga, R. Jackson, and K. Watanabe, J. Quant. Spectry. Radiative Transfer (in press).
10. H. R. Philipp and H. Ehrenreich, Phys. Rev. 131, 2016 (1963).
11. J. C. Phillips, Phys. Rev. Letters 12. (1964).
12. T. Miyakawa, J. Phys. Soc. Japan 17, 1898 (1962).
13. J. C. Phillips, Phys. Rev., 136, A 1705 (1964).
14. J. C. Phillips, Phys. Rev., 136, A 1714 (1964).
15. J. C. Phillips, Phys. Rev., 136, A 1721 (1964).